HHS Public Access

Author manuscript

Dev Neurosci. Author manuscript; available in PMC 2021 April 29.

Published in final edited form as:

Dev Neurosci. 2019 ; 41(5-6): 274–289. doi:10.1159/000506679.

White Matter Alterations in *Fmr1* KO mice during Early Postnatal Brain Development

Da Shi[1,2], **Su Xu**[1], **Jiachen Zhuo**[1], **Mary C. McKenna**[3,4], **Rao P. Gullapalli**[1,2,4]

[1]Department of Diagnostic Radiology and Nuclear Medicine, University of Maryland School of Medicine, Baltimore, MD, USA

[2]Department of Biochemistry and Molecular Biology, University of Maryland School of Medicine, Baltimore, MD, USA

[3]Department of Pediatrics, University of Maryland School of Medicine, Baltimore, MD, USA

[4]Program in Neuroscience, University of Maryland School of Medicine, Baltimore, MD, USA

Abstract

Fragile X syndrome (FXS) is the most commonly inherited form of intellectual disability ascribed to the autism spectrum disorder. Studies with FXS patients have reported altered white matter volume compared to controls. The *Fmr1* knockout mouse (KO), a model for FXS, showed evidence of delayed myelination during postnatal brain development. In this study, we examined several white matter regions in the male *Fmr1* KO mouse brain compared to male wild-type (WT) mice at postnatal days 18 (PND 18), 21, 30 and 60, which coincide with critical stages of myelination and postnatal brain development. White matter volume, T_2 relaxation time, and magnetization transfer ratio (MTR) were measured using magnetic resonance imaging and myelin content was determined with histological staining of myelin. Differences in the developmental accumulation of white matter and myelin between *Fmr1* KO and WT mice were observed in the corpus callosum, external and internal capsules, cerebral peduncle, and fimbria. Alterations were more predominant in the external and internal capsules and fimbria of *Fmr1* KO mice, where the MTR was lower at PND 18, then elevated at PND 30 and again lowered at PND 60 compared to the corresponding regions in WT mice. The pattern of changes in MTR were similar to those observed in myelin staining and could be related to the altered protein synthesis that is a hallmark of FXS. While no significant changes in white matter volumes and T_2-relaxation time between the *Fmr1* KO and WT mice were observed, the altered pattern of myelin staining and MTR,

Contact information: Rao P. Gullapalli, PhD, Professor, Department of Diagnostic Radiology & Nuclear Medicine, 670 W Baltimore St, Rm L127, University of Maryland School of Medicine, Baltimore, MD 21201, Phone: 410-706-2694, Fax: 410-706-1046, rgullapalli@som.umaryland.edu.

Author Contributions

DS performed histological and MRI experiments, data analysis and writing of manuscript.
SX contributed technical and conceptual expertise to MRI and assisted in writing and proofreading of manuscript.
JZ contributed technical and analytical expertise to MRI and assisted in proofreading of manuscript.
MCM contributed to design of the experiments, histological expertise and preparation of manuscript.
RPG contributed to design of the experiments, MRI expertise and preparation of manuscript.

Disclosure Statement

The authors have no conflicts of interests to disclose.

Statement of Ethics:

The Institutional Animal Care and Use Committee at the University of Maryland, Baltimore approved the protocol used in this study.

particularly in the external capsule, reflect the abnormalities associated with myelin content is suggestive of a developmental delay in the white matter of *Fmr1* KO mouse brain. These early differences in white matter during critical developmental stages may contribute to altered brain networks in the *Fmr1* KO mice.

Keywords

Fragile X syndrome; *Fmr1* knockout; magnetization transfer; T_2 relaxation; myelination

Introduction

Fragile X syndrome (FXS) is the most commonly inherited form of sex-linked intellectual disability affecting 1 in 5000 males [1]. FXS causes intellectual disability and behaviors commonly seen in the autism spectrum disorder, including hyperactivity, social anxiety, and attentional problems [1, 2]. FXS is caused by the mutational insertion of CGG trinucleotide repeats which leads to the epigenetic silencing of the *FMR1* gene [3]. The silencing results in the loss of the mRNA binding protein fragile X mental retardation protein (FMRP) [4, 5]. FMRP regulates the translation of mRNAs that are associated with proteins necessary for synaptic function and myelin integrity [6]. Most notably, the loss of FMRP leads to elevated levels of protein synthesis in the brain [7], impaired regulation of neuronal signaling and synaptic plasticity [8–12], and elevated levels of immature dendritic spines in the cortex and hippocampus [13–17]. These alterations may contribute to symptoms associated with FXS [2, 18]. A preclinical model of FXS, the *Fmr1* knockout (KO) mouse [19] is commonly used to study FXS and models many of the clinical manifestations of FXS.

Much of the research in FXS focuses on neuronal changes and neurodevelopmental symptoms [10, 20]. However, astrocyte and oligodendrocyte dysfunction has been reported that may contribute to alterations in brain function associated with the *Fmr1* KO mouse phenotype [21–23]. Astrocytes from *Fmr1* KO mouse brain co-cultured with neurons from normal wild type (WT) mouse brain caused *Fmr1* KO-like neuronal morphology including increased axonal branching and immature dendritic spine density in WT neurons, suggesting astrocytes may contribute to the neuronal phenotype [21, 24, 25]. FMRP binds to mRNAs of myelin proteins including myelin basic protein (MBP) [6, 23], 2’ 3’-cyclic-nucleotide 3’-phosphodiesterase (CNP), proteolipid protein, and myelin-associated glycoprotein [6]. Although the role of FMRP in oligodendrocyte maturation is still unknown; the finding that pre- and immature oligodendrocytes contain FMRP, and levels are greatly reduced in mature oligodendrocytes suggests a developmental role for FMRP [23, 26]. MBP is an abundant protein that ensures the stability of myelin sheaths [27]. Evidence of delayed myelination has been reported in the cerebellar white matter of postnatal *Fmr1* KO mice, including reduced myelin thickness and reduced concentrations of MBP and CNP at PND 7, all of which were normalized at PND 30 compared to WT mice [22]. Altered MBP levels at different postnatal ages suggest that the loss of FMRP regulation of MBP mRNA may have long term consequences with respect to myelin integrity in *Fmr1* KO mouse brain [22].

Imaging studies of *Fmr1* KO mouse brain revealed differences in regional brain volume, including an increase in hippocampal [28] and a decrease in cerebellar [22] volumes, as well as changes in brain metabolite concentrations that may influence myelination [28, 29]. In children with FXS, greater overall white matter volume and alterations of regional white matter volumes during brain development have been reported [30, 31]. Taken together, these studies provide evidence that alterations in white matter development may contribute to altered neurodevelopment associated with FXS. However, very little has been done to characterize the underlying alterations associated with changes in brain volume using advanced imaging techniques in FXS patients and *Fmr1* KO mouse brain.

In this study we hypothesized decreased myelin levels are found in white matter during brain postnatal development in *Fmr1* KO mice compared to the WT mice. Measurements were taken at critical time points in the course of myelination and neural network development, with PND 18 being before, and PND 21 during the peak of myelination and synaptogenesis in rodents [32]. Additionally, ages that coincide with previous reports of neural network development at PND 30 and maturation at PND 60 were also studied [32]. Using magnetization transfer and T_2 imaging, we assessed microstructural white matter development in the corpus callosum, external capsule, internal capsule, cerebral peduncle and hippocampal fimbria *ex vivo* in perfused brains from *Fmr1* KO and WT mice. Histological staining was used to quantify myelin and verify results from T_2 relaxation time and magnetization transfer imaging.

Methods and Materials

Animal procedure

Fmr1 KO mice (JAX B6.129P2-fmr1^{tmICgr} mice; Jackson Laboratory, Bar Harbor, ME, USA) from a C57Bl6J background were bred in the animal facility at the University of Maryland, Baltimore. The *Fmr1* KO mice were generated by hemizygous mating of *Fmr1* KO female to *Fmr1* KO males. The WT mice were generated by homozygous mating of the WT female to the WT male. The *Fmr1* KO mice were backcrossed for more than 10 generations. The Institutional Animal Care and Use Committee at the University of Maryland, Baltimore approved the protocol used in this study. All mice were weaned at PND 21. Food and water were given ad libitum.

Mice were studied at PND 18 (9 *Fmr1* KO, 9 WT), PND 21 (12 *Fmr1* KO, 14 WT), PND 30 (13 *Fmr1* KO, 12 WT), and PND 60 (6 *Fmr1* KO, 6 WT). Once animals reached the appropriate age, the male *Fmr1* KO and WT mice were anesthetized with 4% isoflurane and perfused through the left ventricle with phosphate buffered saline (PBS), followed by 4% paraformaldehyde fixative. The whole brain was removed from the skull to ensure the brain was completely fixed before imaging and immersed in fixative for 48 hours. It was decided to excise the brain from the skull to ensure fixation of white matter structure and extra precaution was made to prevent damage to the forebrain and midbrain during dissection. The fixed brain was then immersed in PBS for one week to minimize the effect of the fixative on T_2 relaxation time and magnetization transfer ratio (MTR) [33, 34]. The fixation procedure was tightly controlled to minimize any variations associated with tissue processing. These fixed brains were used in order to detect subtle changes between white matter of *Fmr1* KO

and WT mice using MRI. The fixed brains were placed in a customized conical tube filled with a proton-free susceptibility-matching fluid Fluorinert (3M, St. Paul, MN) prior to MR imaging. Fluorinert does not degrade the sample because it is biologically inert [35] and has been safely used for *in vivo* molecular imaging [36].

Magnetic resonance imaging

MRI techniques used in this study are commonly used to characterize developmental and pathological changes in white matter because they are sensitive to the chemical and physical environments of water protons [37–40]. All experiments were performed on a Bruker Biospec 7.0 Tesla 30 cm horizontal bore scanner (Bruker Biospin MRI, Ettlingen, Germany) using Paravision 5.1 software. A Bruker 72-mm linear-volume coil as the transmitter and a four-channel Bruker ^{1}H surface array coil as the receiver were used for imaging. Prior to imaging, magnetic field inhomogeneity was adjusted using the FASTMAP technique [41]. Anatomical images were obtained using a 3D TurboRARE sequence covering a slab of 15 mm in thickness over the whole brain, from the forebrain to the hindbrain, to obtain T_2-weighted images at a spatial resolution of 113 μm X 150 μm X 170 μm, using an echo time (TE) and repeat time (TR) of 11 milliseconds (ms) and 2500 ms, respectively, with two averages.

Transverse relaxation time T_2 values decrease with the extent of myelination in white matter [42]. Quantitative information on T_2-relaxation time was obtained using an eight echo, multi-echo spin echo sequence with three continuous slices centered on the hippocampus at Bregma −1.82, without any gap. The spatial resolution was 200 μm X 200 μm, acquired with 1 mm slice thickness, TEs of 9.3, 27.9, 46.5, 65.1, 83.7, 102.3, 120.9, and 139.5 ms at a TR of 10000 ms, and two averages.

Changes in the relative levels of macromolecules can be detected using magnetization transfer, a technique that exploits the exchange between the bound protons in the macromolecules and the protons in free water, providing a contrast that is reflective of the concentration of macromolecules present in tissue [43–46]. In white matter, such a contrast would be indicative of myelin water content since myelin macromolecules such as lipids and proteins serve as the major pool of bound protons. Thus, magnetization transfer imaging provides an index of relative content of macromolecules in white matter, and is reported as MTR [38, 45, 46].

The magnetization transfer images were obtained using a fast low shot (FLASH) T_1 technique. Acquisition parameters were slice thickness 0.5 mm, 0.5 mm gap, 16 slices that covered the cerebral cortex and the cerebellum, spatial resolution of 200 μm X 200 μm over a field of view of 1.5 cm X 1.5 cm, TE/TR = 3.6/280 ms, and 32 averages. For the magnetization transfer images (M_s), a Gaussian off-resonance saturation pulse was used with duration of 12.6 ms and flip angle of 180 degrees at an off-resonance frequency of 5000 Hz from the center frequency of water protons. The reference magnetization transfer image (M_o) was scanned using the same parameters except without the off-resonance pulse.

Image Processing

Images were transferred offline to an independent database for further processing. Medical Image Processing, Analysis and Visualization tool (MIPAV v5.3.1, CIT; NIH, Bethesda, MD, USA) was used to obtain volumes of different regions and to extract information for computing the MTR. Regions of interest (ROIs) were drawn manually on both the 3D T_2 anatomical and magnetization transfer images by comparison with an anatomical reference atlas [47]. The image contrast was not clear enough for automatic segmentation at early ages; therefore the ROIs were drawn by one operator for consistency. ROIs included the whole brain, corpus callosum, external capsule, internal capsule, cerebral peduncle, and fimbria. Both absolute and normalized white matter volume was obtained by dividing each regional white matter volume by whole brain volume. MTR was calculated as $[(M_0\text{-}M_s) / M_0] \text{ X } 100$, where M_0 is the signal intensity from images obtained without the off-resonance pulse and M_s is the signal intensity from images where the saturation pulse was applied [45]. T_2-relaxation time was measured using an in-house Matlab program [48]. The data from all echo times for each ROI were fitted to a mono-exponential decay curve. The first echo at 9.3 ms was ignored to minimize potential contamination from the stimulated echo. The volumes, T_2-relaxation times, and MTR values from each ROI were obtained and analyzed for statistically significant differences.

Histology

Following MRI, six of the perfused brains from each genotype and age were placed in 30% sucrose solution for cryoprotection. Brains were then frozen and coronal sections 40 μm in thickness were prepared with a cryostat at −20°C. One section was collected from every 12 sections, approximately 0.50 mm apart. Sections were stained for myelin with Black Gold II (EMD Millipore, Billerica, MA) by the following procedure described by Schmued et al. [49]. Mounted slides were rehydrated with two washes of de-ionized water, followed by staining with 0.3% Black Gold II in saline solution at 60°C. After staining was complete, the slides were washed in 1% sodium thiosulfate solution at 60°C followed by three washes in water at room temperature [49]. Images were taken on a brightfield Olympus BX53 microscope at 10X magnification and analyzed using Bioquant Life Sciences 2013 v13.5.6 software (Bioquant Image Analysis Inc. Nashville, TN). A white field correction was applied to all images prior to obtaining optical density. The red channel was used to determine density because Black Gold II stains myelinated fibers red-brown. The intensity of myelin staining in white matter regions was measured as optical density. The optical density was calculated as the log of the intensity of the ROI divided by the intensity of the background [50]. The optical density value was normalized to the area (in μm^2) of the ROI. Optical densities were measured between Bregma 0.50 mm to −2.46 mm which included 5–6 sections of the corpus callosum and external capsule, 1–2 sections with the internal capsule, 2–3 sections for cerebral peduncle, and 3–4 sections for the fimbria. The ROIs selected for histology were matched with anatomical references by Franklin and Paxinos [47] during ROI selection and number of ROIs were adjusted to with age to cover similar white matter regions throughout the forebrain and midbrain. While the number of brains used for histology were less than the number of brains imaged, each brain were randomly selected among the litter group to avoid litter effect and bias.

Statistical Analysis

All statistical analyses were performed in SPSS (IBM Corp. 2013. IBM SPSS Statistics for Windows, Version 22.0. Armonk, NY). A separate two-way analysis of variance (ANOVA) was performed for each region in each parameter, including volume, normalized volume, MTR, T_2 relaxation, and optical density. Each two-way ANOVA compared the effect of genotype, age, and the interaction of (genotype X age). Genotype and age effects were analyzed by Student's t-tests if the interaction between factors was statistically significant ($p < 0.05$). To control for multiple pairwise comparisons, a false discovery rate with threshold of alpha = 0.05 was performed on the p-values. The threshold assumes 5% of significant p-values may be false positives, and if a significant p-value does not pass false discovery rate then that p-value may be a false positive.

Results

White matter volumes

Representative images of the fixed brain are shown in Figure 1a for each age and genotype. Additionally, Figure 1a shows representative image of the drawn white matter ROIs from WT PND 30 mouse brain. No differences in regional white matter or whole brain volumes were found between *Fmr1* KO and WT mice (Figure 1, Table 1). The white matter volume normalized to whole brain volume was also not significantly different between *Fmr1* KO and WT mice (Table 2). Significant effect of age was observed in all white matter regions studied and the white matter volume increased with age (Figure 1 and Table 1). The (genotype X age) interaction was not statistically significant in the whole brain and regional white matter volumes (Table 1), as well as with normalized regional white matter volumes (Table 2), indicating that the developmental courses of change in white matter volumes were similar between the two genotypes.

T_2-relaxation time

T_2-relaxation time can provide insights into white matter environment and generally decreases following development of white matter [42]. Representative T_2 images at TE = 9.3ms are shown in Figure 2a for each age and genotype. T_2-relaxation time was measured in the corpus callosum, external capsule, internal capsule, cerebral peduncle, and fimbria of brains from *Fmr1* KO and WT mice (Figure 2b–f, respectively). The (genotype X age) interaction was not statistically significant in the white matter regions studied (Table 1) indicating that changes in T_2-relaxation time over the course of development were not different between the two genotypes. The significant effect of age in the corpus callosum, external capsule, and fimbria is indicative of developmental decrease in T_2-relaxation times [42] (Table 1). These trends in white matter regions of WT mice showed decreased T_2-relaxation times between PND 18 and PND 30 as expected over the course of myelination. In *Fmr1* KO mice, however, T_2-relaxation time decreased more sharply in the corpus callosum, external capsule, and fimbria between PND 21 and PND 30, suggesting delayed patterns in myelination. It should be noted that poor signal to noise prevented analysis of one *Fmr1* KO mouse brain at PND 30.

Magnetization Transfer Ratio

MTR is considered to be an index of macromolecular content in white matter, including myelin proteins and lipids that contribute to the structural integrity of white matter [38]. MTR detected differences in macromolecular content, indicative of differences in white matter maturation of *Fmr1* KO mouse brain compared to WT brain (Figure 3). Figure 3a shows representative images at the center frequency of water protons for *Fmr1* KO and WT mouse brains at PNDs 18, 21, 30, and 60. Significant (genotype X age) interaction was found in MTR data for all white matter regions studied (Table 1). In WT mice, MTR tended to be fairly level between PND 18 and PND 30 and increased thereafter (Figure 3). At PND 60 when the brain networks are more mature [32], MTR in all regions examined was higher in WT compared to *Fmr1* KO mice (Figure 3). Before the peak of myelination at PND 18, MTR in the white matter regions of *Fmr1* KO mice was lower in the internal capsule ($t(2.56)$ $p<0.05$), cerebral peduncle ($t(2.41)$ $p<0.05$), fimbria ($t(2.42)$ $p<0.05$), and cerebellar white matter ($t(2.58)$ $p<0.05$) (Figure 3d, e, f, and g respectively) compared to WT mice. MTR in *Fmr1* KO mouse brain showed a steep increase between PND 18 and PND 30 followed by a decrease or leveling off between PND 30 and PND 60 (Figure 3). No differences were found at PND 21. At PND 30, during a period when the neural networks begin to establish along with continued myelination in the mouse brain [32], the internal capsule ($t(2.21)$, $p<0.05$) and fimbria ($t(2.33)$, $p<0.05$) showed significantly higher MTR in *Fmr1* KO mouse brains compared to the WT (Figure 3d and 3f, respectively). At PND 60 when the brain networks are more mature [32], lower MTR was observed in the corpus callosum ($t(2.29)$ $p<0.05$), external capsule ($t(2.54)$ $p<0.05$) and internal capsule ($t(2.27)$ $p<0.05$) in *Fmr1* KO mouse brains compared to the WT (Figure 3b, 3c, and 3d, respectively). The significant p-values from multiple pairwise comparisons passed false discovery rate with a threshold of alpha = 0.05. The developmental differences in MTR between *Fmr1* KO and WT mouse brains suggested a lower content of myelin proteins and/or lipids at PND 18 and 60 in the white matter of *Fmr1* KO mouse brain. Overall, alterations in MTR are suggestive of fluctuation in macromolecule content during development in the *Fmr1* KO mouse brain that may have an impact on stable myelin structure formation.

Myelin staining

To directly determine myelin content in brain we stained tissue with Black Gold II, a histological stain for myelin [49]. Figure 4a shows the myelin staining of a representative section from *Fmr1* KO mouse brain and WT mouse brain at each age. Myelin density measured from Black Gold II staining showed significant interaction of (genotype X age) in the external capsule, internal capsule, cerebral peduncle and fimbria (Table 1). The myelin density was lower in *Fmr1* KO mouse brain at PND 18 in the external capsule ($t(6.88)$, $p<0.001$), internal capsule ($t(3.50)$, $p<0.001$), and fimbria ($t(2.01)$, $p<0.05$) compared to the corresponding regions of WT mouse brain (Figure 4c, d, and f, respectively). Myelin density at PND 21 was elevated in the cerebral peduncle of *Fmr1* KO mouse brain compared to WT ($t(2.10)$, $p<0.05$) (Figure 4e). By PND 30, the myelin density was elevated in many white matter regions of the *Fmr1* KO mouse brain, including the external capsule ($t(4.82)$, $p<0.001$), internal capsule ($t(2.11)$, $p<0.05$), and fimbria ($t(4.61)$, $p<0.001$) when compared to the corresponding regions of WT mouse brain (Figure 4c, d, and f, respectively). At PND 60 the myelin density in *Fmr1* KO mouse brain was lower in the external capsule ($t(6.61)$,

p<0.001) compared to the WT brain (Figure 4c). The significant p-values passed false discovery rate (alpha = 0.05) for multiple pairwise comparisons.

The myelin density in the white matter regions of *Fmr1* KO mice showed different developmental time courses than the WT mice (Figure 4). In WT brain, myelin density increased steeply between PND 30 and PND 60 in the corpus callosum and external capsule; whereas, in the corresponding regions of *Fmr1* KO brain the increase in myelin density occurred between PND 18 and PND 30 and tended to level off thereafter. The myelin densities of internal capsule, cerebral peduncle and hippocampal fimbria in WT brain increased steadily from PND 18 to PND 60; whereas, in *Fmr1* KO brain the myelin density increased more gradually from PND 18 to 60. The myelin density in the external and internal capsules showed similar trends as the MTR results, where *Fmr1* KO mouse showed lowered myelin density at PND 18 followed by elevated levels at PND 30 which was reduced at PND 60 compared to the corresponding regions of WT mouse brain (Figure 4).

Discussion

Myelination delay in white matter in the developing *Fmr1* KO mouse

Myelination of axons in normally developing human brains starts prenatally and undergoes conspicuous growth during the first two years of life [51], then continues to increase at a lower rate from childhood into early adulthood, and declines in late adulthood [52, 53]. In comparison, the peak of myelination in the normally developing rodent brain occurs between PND 20–21 [32], grows steadily at a reduced rate throughout adulthood and declines around 18 months of age [32, 52, 53]. Moreover, the developmental process of myelination varies regionally [54].

Our results demonstrate an abnormal pattern of accumulation of macromolecules determined by MTR and myelin staining during early postnatal development in brains of *Fmr1* KO mice compared to brains of WT mice (Figures 3 and 4). The results of MTR and the myelin density measurements show similar trends in the *Fmr1* KO mouse brain, suggesting that histological changes in myelin density correspond closely with MTR in the fixed brain. In the present study, the differences in myelin density and MTR at PND 18, 30 and 60 in the *Fmr1* KO mice compared to WT suggests that alterations in forebrain and midbrain white matter, most notably in the external and internal capsules occur throughout postnatal brain development including before peak of myelination at PND 18, and during development and maturation of the neural networks at PND 30 and PND 60, respectively.

Reduced myelin thickness has been reported in the cerebellar white matter of *Fmr1* KO mice at PND 7, although differences were not observed at PND 15 or older ages [22]. However, reduced rates of myelination or delayed myelination may also be present at older ages, which could explain lowered MTR and myelin density at PND 18 and PND 60 found in white matter regions of the current study. Magnetization transfer imaging is sensitive to the macromolecules in white matter, particularly the proteins and lipids in myelin [55]. Previous in-depth research demonstrated that cholesterol and myelin lipids contribute significantly to the magnetization transfer effect [55, 56]. The MTR from the present study suggests altered levels of white matter macromolecules, including lipids and proteins, at different stages of

brain development that could contribute to altered myelin composition in *Fmr1* KO mice. When placed in context with myelin staining, the most prominent differences were alterations during the developmental phase of the internal capsule and later in the external capsule in the maturing *Fmr1* KO mice brains. The alteration in myelin composition and density during brain development suggests that the process of myelination is dysregulated during development in *Fmr1* KO brain, which could adversely influence neuronal function and potentially have a negative impact on the formation and maturation of brain networks. Future studies in the mouse model will incorporate *in vivo* functional imaging methods in *Fmr1* KO mice at the critical developmental ages revealed from the current studied.

Reduced MTR has been associated with pathological states of demyelination and axonal degeneration in patients with and in preclinical models of multiple sclerosis [37, 39, 40]. In an animal model of multiple sclerosis, lower MTR was found in the corpus callosum and external capsule of mice treated with cuprizone, an agent that caused demyelination [39]. It is important to note that similar MTR values were found for *in vivo* and *ex vivo* imaging of the mouse model of multiple sclerosis by Thiessen et al. [39].

A previous study with the MBP deficient Shiverer mouse revealed no differences in Black Gold II staining compared to controls, suggesting that Black Gold II staining of myelin may have greater specificity to lipids [57]. Therefore, altered MTR and myelin staining in *Fmr1* KO mouse brain likely reflects differences in lipid content because myelin composition is composed of 70–85% lipids [54]. Thus, the similar trends between MTR and myelin density data from the present study suggest alterations in lipid levels in the developing *Fmr1* KO mouse brain, in addition to altered myelin protein levels reported by Pacey et al. [22]. A recent study reported reduced plasma cholesterol and reduced low and high-density lipoproteins in male FXS patients (4–20+ years) compared to the normal control population [58]. Although it has not been determined whether brain cholesterol levels might be altered in FXS patients or *Fmr1* KO mice, cholesterol is known to be heavily incorporated into myelin particularly during the peak of myelination in the normal brain [59] and the cholesterol utilized for myelination is mainly synthesized in the brain [60]. Furthermore, an overall cholesterol deficiency could contribute to impaired neurotransmission and has been associated with neurodegenerative diseases [61]. Thus, the lowered MTR and myelin density found in white matter of *Fmr1* KO mice may be due to decreased lipids and also the lack of FMRP regulation on the mRNA levels and synthesis of myelin proteins [6] which may lead to delayed myelination as observed in the present study.

White matter volume in the FXS brain

Numerous MRI studies have reported alterations in brain volumes of young and adolescent FXS patients, including changes in regional gray and white matter volumes of cortical and subcortical regions, compared to normally developing children [30, 31, 64, 65]. Although the current findings do not show consistent differences in white matter volume between *Fmr1* KO and WT mouse brains, our data agree with a recent study that reported no difference in white matter volumes of the corpus callosum, internal capsule and fimbria in fixed C57Bl6J *Fmr1* KO mouse brain compared to WT at PND 60 [63]. An earlier *in vivo* study from our group found increased volume of the hippocampus in *Fmr1* KO brains

compared to WT brains [28]. The C57Bl6J strain of *Fmr1* KO mouse was chosen for this study because it is a widely used model of FXS [15, 16, 62] and a previous study demonstrating delayed myelination also used this model [22]. Although white matter volumes were not changed, the magnetization transfer imaging technique used in this study showed evidence of alterations in myelin and white matter in developing *Fmr1* KO mice.

Imaging the fixed brain

The imaging findings along with results from myelin staining suggest that magnetization transfer imaging may be particularly useful to better understand the microstructure of white matter in FXS brain *in vivo*. However, the current findings have to be taken in context of the limitations of the study. It is likely that the T_2 and MTR values measured *in vivo* may be different from those measured in a fixed tissue sample because the fixative solution has been shown to affect the T_2 and MTR values compared to *in vivo* measurements [33, 34]. In the present study precautions were taken to minimize the effect of fixative in T_2 relaxation and MTR in the fixed brain, based on published studies of fixed and *in vivo* brain samples [33, 34]. In addition, it has been shown that the data trends from fixed samples are similar to *in vivo* with T_2 [34] and with MTR following immersion of PFA fixed brain tissue in PBS [39].

Our goal in this study was to obtain an accurate assessment of any subtle changes in white matter development by obtaining high-resolution volumetric, T_2, and MTR data. Thus, we elected to perform these measurements on fixed brains to stabilize brain structure, allow longer imaging durations and eliminate confounds of any motion artifacts as with in previous studies [22, 29, 63]. The findings of the current study regarding the utility of MTR in revealing developmental changes in *Fmr1* KO mouse are compelling. Future studies should focus on using MTR in conjunction with other advanced MRI techniques *in vivo* to assess their utility as imaging markers for FXS and also to assess whether such changes alter brain connectivity in *Fmr1* KO mouse.

Conclusions

In this study, we found altered levels of myelin and macromolecules in the white matter of *Fmr1* KO mouse brain at key developmental ages compared to the corresponding regions of WT mouse brain. We observed delayed myelination before the peak of myelination at PND 18, and then increased myelin density at PND 30 suggesting compensation for the delayed myelination, followed by lowered myelin levels in adult *Fmr1* KO mouse brain compared to WT mouse brain. Differences in white matter and myelin between *Fmr1* KO and WT mouse brains were found at several ages during development and could potentially contribute to changes in the brain networks of *Fmr1* KO mouse. Alterations in white matter and myelin that coincided with key stages of brain development including early myelination, the peak of myelination and synaptogenesis, neural network development and maturation in mouse brain suggest dysregulation of myelination and white matter maturation in *Fmr1* KO mouse brain during development and suggest complex differences in white matter development which may ultimately result in altered brain function.

Acknowledgements

The authors thank Dr. Jaylyn Waddell, Dr. Shiyu Tang, and Dr. Carolyn B. Smith for their advice and assistance with statistics.

Funding Sources

This study was supported by the Core for Translational Imaging @ Maryland (C-TRIM) which part of the University of Maryland School of Medicine Center for Innovative Biomedical Resources in Baltimore, the FRAXA Research Foundation, and NIH P01 grant HD016596 (MCM).

References

1. Coffee B, Keith K, Albizua I, Malone T, Mowrey J, Sherman SL, et al. Incidence of fragile X syndrome by newborn screening for methylated FMR1 DNA. Am J Hum Genet. 2009;85(4):503–14. [PubMed: 19804849]
2. Garber KB, Visootsak J, Warren ST. Fragile X syndrome. Eur J Hum Genet. 2008;16(6):666–72. [PubMed: 18398441]
3. Verkerk AJ, Pieretti M, Sutcliffe JS, Fu YH, Kuhl DP, Pizzuti A, et al. Identification of a gene (FMR-1) containing a CGG repeat coincident with a breakpoint cluster region exhibiting length variation in fragile X syndrome. Cell. 1991;65(5):905–14. [PubMed: 1710175]
4. Ashley CT, Jr, Wilkinson KD, Reines D, Warren ST. FMR1 protein: conserved RNP family domains and selective RNA binding. Science. 1993;262(5133):563–6. [PubMed: 7692601]
5. Devys D, Lutz Y, Rouyer N, Bellocq JP, Mandel JL. The FMR-1 protein is cytoplasmic, most abundant in neurons and appears normal in carriers of a fragile X premutation. Nat Genet. 1993;4(4):335–40. [PubMed: 8401578]
6. Darnell JC, Van Driesche SJ, Zhang C, Hung KY, Mele A, Fraser CE, et al. FMRP stalls ribosomal translocation on mRNAs linked to synaptic function and autism. Cell. 2011;146(2):247–61. [PubMed: 21784246]
7. Qin M, Kang J, Burlin TV, Jiang C, Smith CB. Postadolescent changes in regional cerebral protein synthesis: an in vivo study in the FMR1 null mouse. J Neurosci. 2005;25(20):5087–95. [PubMed: 15901791]
8. Paluszkiewicz SM, Martin BS, Huntsman MM. Fragile X syndrome: the GABAergic system and circuit dysfunction. Dev Neurosci. 2011;33(5):349–64. [PubMed: 21934270]
9. Gross C, Berry-Kravis EM, Bassell GJ. Therapeutic strategies in fragile X syndrome: dysregulated mGluR signaling and beyond. Neuropsychopharmacology. 2012;37(1):178–95. [PubMed: 21796106]
10. Hagerman R, Lauterborn J, Au J, Berry-Kravis E. Fragile X syndrome and targeted treatment trials. Results Probl Cell Differ. 2012;54:297–335. [PubMed: 22009360]
11. Martin BS, Huntsman MM. Pathological plasticity in fragile X syndrome. Neural Plast. 2012;2012:275630. [PubMed: 22811939]
12. Cea-Del Rio CA, Huntsman MM. The contribution of inhibitory interneurons to circuit dysfunction in Fragile X Syndrome. Front Cell Neurosci. 2014;8:245. [PubMed: 25202236]
13. Irwin SA, Galvez R, Greenough WT. Dendritic spine structural anomalies in fragile-X mental retardation syndrome. Cereb Cortex. 2000;10(10):1038–44. [PubMed: 11007554]
14. Irwin SA, Idupulapati M, Gilbert ME, Harris JB, Chakravarti AB, Rogers EJ, et al. Dendritic spine and dendritic field characteristics of layer V pyramidal neurons in the visual cortex of fragile-X knockout mice. Am J Med Genet. 2002;111(2):140–6. [PubMed: 12210340]
15. Bilousova TV, Dansie L, Ngo M, Aye J, Charles JR, Ethell DW, et al. Minocycline promotes dendritic spine maturation and improves behavioural performance in the fragile X mouse model. J Med Genet. 2009;46(2):94–102. [PubMed: 18835858]
16. Grossman AW, Aldridge GM, Lee KJ, Zeman MK, Jun CS, Azam HS, et al. Developmental characteristics of dendritic spines in the dentate gyrus of Fmr1 knockout mice. Brain Res. 2010;1355:221–7. [PubMed: 20682298]

17. Pan F, Aldridge GM, Greenough WT, Gan WB. Dendritic spine instability and insensitivity to modulation by sensory experience in a mouse model of fragile X syndrome. Proc Natl Acad Sci U S A. 2010;107(41):17768–73. [PubMed: 20861447]
18. Kidd SA, Lachiewicz A, Barbouth D, Blitz RK, Delahunty C, McBrien D, et al. Fragile X syndrome: a review of associated medical problems. Pediatrics. 2014;134(5):995–1005. [PubMed: 25287458]
19. Bakker C Fmr1 knockout mice: a model to study fragile X mental retardation. The Dutch-Belgian Fragile X Consortium. Cell. 1994;78(1):23–33. [PubMed: 8033209]
20. Berry-Kravis E, Sumis A, Hervey C, Mathur S. Clinic-based retrospective analysis of psychopharmacology for behavior in fragile x syndrome. Int J Pediatr. 2012;2012:843016. [PubMed: 22899942]
21. Jacobs S, Doering LC. Astrocytes prevent abnormal neuronal development in the fragile x mouse. J Neurosci. 2010;30(12):4508–14. [PubMed: 20335488]
22. Pacey LK, Xuan IC, Guan S, Sussman D, Henkelman RM, Chen Y, et al. Delayed myelination in a mouse model of fragile X syndrome. Hum Mol Genet. 2013;22(19):3920–30. [PubMed: 23740941]
23. Wang H, Ku L, Osterhout DJ, Li W, Ahmadian A, Liang Z, et al. Developmentally-programmed FMRP expression in oligodendrocytes: a potential role of FMRP in regulating translation in oligodendroglia progenitors. Hum Mol Genet. 2004;13(1):79–89. [PubMed: 14613971]
24. Jacobs S, Cheng C, Doering LC. Hippocampal neuronal subtypes develop abnormal dendritic arbors in the presence of Fragile X astrocytes. Neuroscience. 2016;324:202–17. [PubMed: 26968765]
25. Jacobs S, Nathwani M, Doering LC. Fragile X astrocytes induce developmental delays in dendrite maturation and synaptic protein expression. BMC Neurosci. 2010;11:132. [PubMed: 20955577]
26. Gholizadeh S, Halder SK, Hampson DR. Expression of fragile X mental retardation protein in neurons and glia of the developing and adult mouse brain. Brain Res. 2015;1596:22–30. [PubMed: 25446451]
27. Harauz G, Ladizhansky V, Boggs JM. Structural polymorphism and multifunctionality of myelin basic protein. Biochemistry. 2009;48(34):8094–104. [PubMed: 19642704]
28. Shi D, Xu S, Waddell J, Scafidi S, Roys S, Gullapalli RP, et al. Longitudinal in vivo developmental changes of metabolites in the hippocampus of Fmr1 knockout mice. J Neurochem. 2012;123(6):971–81. [PubMed: 23046047]
29. Ellegood J, Pacey LK, Hampson DR, Lerch JP, Henkelman RM. Anatomical phenotyping in a mouse model of fragile X syndrome with magnetic resonance imaging. Neuroimage. 2010;53(3):1023–9. [PubMed: 20304074]
30. Hazlett HC, Poe MD, Lightbody AA, Styner M, MacFall JR, Reiss AL, et al. Trajectories of early brain volume development in fragile X syndrome and autism. J Am Acad Child Adolesc Psychiatry. 2012;51(9):921–33. [PubMed: 22917205]
31. Hoeft F, Carter JC, Lightbody AA, Cody Hazlett H, Piven J, Reiss AL. Region-specific alterations in brain development in one- to three-year-old boys with fragile X syndrome. Proc Natl Acad Sci U S A. 2010;107(20):9335–9. [PubMed: 20439717]
32. Semple BD, Blomgren K, Gimlin K, Ferriero DM, Noble-Haeusslein LJ. Brain development in rodents and humans: Identifying benchmarks of maturation and vulnerability to injury across species. Prog Neurobiol. 2013;106–107:1–16.
33. Schmierer K, Wheeler-Kingshott CA, Tozer DJ, Boulby PA, Parkes HG, Yousry TA, et al. Quantitative magnetic resonance of postmortem multiple sclerosis brain before and after fixation. Magnetic resonance in medicine. 2008;59(2):268–77. [PubMed: 18228601]
34. Shepherd TM, Thelwall PE, Stanisz GJ, Blackband SJ. Aldehyde fixative solutions alter the water relaxation and diffusion properties of nervous tissue. Magnetic resonance in medicine. 2009;62(1):26–34. [PubMed: 19353660]
35. Flaim SF. Pharmacokinetics and side effects of perfluorocarbon-based blood substitutes. Artificial cells, blood substitutes, and immobilization biotechnology. 1994;22(4):1043–54.

36. Giraudeau C, Geffroy F, Meriaux S, Boumezbeur F, Robert P, Port M, et al. 19F molecular MR imaging for detection of brain tumor angiogenesis: in vivo validation using targeted PFOB nanoparticles. Angiogenesis. 2013;16(1):171–9. [PubMed: 23053783]
37. Schmierer K, Scaravilli F, Altmann DR, Barker GJ, Miller DH. Magnetization transfer ratio and myelin in postmortem multiple sclerosis brain. Ann Neurol. 2004;56(3):407–15. [PubMed: 15349868]
38. Wozniak JR, Lim KO. Advances in white matter imaging: a review of in vivo magnetic resonance methodologies and their applicability to the study of development and aging. Neurosci Biobehav Rev. 2006;30(6):762–74. [PubMed: 16890990]
39. Thiessen JD, Zhang Y, Zhang H, Wang L, Buist R, Del Bigio MR, et al. Quantitative MRI and ultrastructural examination of the cuprizone mouse model of demyelination. NMR in biomedicine. 2013;26(11):1562–81. [PubMed: 23943390]
40. Bonnier G, Roche A, Romascano D, Simioni S, Meskaldji D, Rotzinger D, et al. Advanced MRI unravels the nature of tissue alterations in early multiple sclerosis. Annals of clinical and translational neurology. 2014;1(6):423–32. [PubMed: 25356412]
41. Gruetter R Automatic, localized in vivo adjustment of all first- and second-order shim coils. Magnetic resonance in medicine. 1993;29(6):804–11. [PubMed: 8350724]
42. Paus T, Collins DL, Evans AC, Leonard G, Pike B, Zijdenbos A. Maturation of white matter in the human brain: a review of magnetic resonance studies. Brain Res Bull. 2001;54(3):255–66. [PubMed: 11287130]
43. Finelli DA. Magnetization transfer in neuroimaging. Magnetic resonance imaging clinics of North America. 1998;6(1):31–52. [PubMed: 9449739]
44. Finelli DA, Hurst GC, Amantia P Jr., Gullapali RP, Apicella A. Cerebral white matter: technical development and clinical applications of effective magnetization transfer (MT) power concepts for high-power, thin-section, quantitative MT examinations. Radiology. 1996;199(1):219–26. [PubMed: 8633148]
45. Henkelman RM, Stanisz GJ, Graham SJ. Magnetization transfer in MRI: a review. NMR in biomedicine. 2001;14(2):57–64. [PubMed: 11320533]
46. Wolff SD, Balaban RS. Magnetization transfer contrast (MTC) and tissue water proton relaxation in vivo. Magnetic resonance in medicine. 1989;10(1):135–44. [PubMed: 2547135]
47. Franklin KP, G. The Mouse Brain in Steretaxic Coordinates: Academic Press; 2007.
48. Mullins RJ, Xu S, Pereira EF, Mamczarz J, Albuquerque EX, Gullapalli RP. Delayed hippocampal effects from a single exposure of prepubertal guinea pigs to sub-lethal dose of chlorpyrifos: a magnetic resonance imaging and spectroscopy study. Neurotoxicology. 2013;36:42–8. [PubMed: 23411083]
49. Schmued L, Bowyer J, Cozart M, Heard D, Binienda Z, Paule M. Introducing Black-Gold II, a highly soluble gold phosphate complex with several unique advantages for the histochemical localization of myelin. Brain Res. 2008;1229:210–7. [PubMed: 18657520]
50. Kayser K, Liewald F, Kremer K, Tacke M. Integrated optical density (IOD), syntactic structure analysis, and survival in operated lung carcinoma patients. Pathology, research and practice. 1994;190(11):1031–8.
51. Kinney HC, Brody BA, Kloman AS, Gilles FH. Sequence of central nervous system myelination in human infancy. II. Patterns of myelination in autopsied infants. J Neuropathol Exp Neurol. 1988;47(3):217–34. [PubMed: 3367155]
52. Andersen SL. Trajectories of brain development: point of vulnerability or window of opportunity? Neurosci Biobehav Rev 2003;27(1–2):3–18. [PubMed: 12732219]
53. Xie F, Zhang JC, Fu H, Chen J. Age-related decline of myelin proteins is highly correlated with activation of astrocytes and microglia in the rat CNS. Int J Mol Med. 2013;32(5):1021–8. [PubMed: 24026164]
54. Quarles RHMW, Morell P. Myelin Formation, Structure and Biochemistry Basic Neurochemistry: Molecular, Cellular and Medical Aspects. 8th edition: Academic Press, Inc.; 2012 p. 51.
55. Stanisz GJ, Kecojevic A, Bronskill MJ, Henkelman RM. Characterizing white matter with magnetization transfer and T(2). Magnetic resonance in medicine. 1999;42(6):1128–36. [PubMed: 10571935]

56. Koenig SH. Cholesterol of myelin is the determinant of gray-white contrast in MRI of brain. Magnetic resonance in medicine. 1991;20(2):285–91. [PubMed: 1775053]
57. Savaskan NE, Weinmann O, Heimrich B, Eyupoglu IY. High resolution neurochemical gold staining method for myelin in peripheral and central nervous system at the light- and electron-microscopic level. Cell Tissue Res. 2009;337(2):213–21. [PubMed: 19513756]
58. Berry-Kravis E, Levin R, Shah H, Mathur S, Darnell JC, Ouyang B. Cholesterol levels in fragile X syndrome. Am J Med Genet A. 2015;167A(2):379–84. [PubMed: 25424470]
59. Saher G, Brugger B, Lappe-Siefke C, Mobius W, Tozawa R, Wehr MC, et al. High cholesterol level is essential for myelin membrane growth. Nat Neurosci. 2005;8(4):468–75. [PubMed: 15793579]
60. Jurevics H, Morell P. Cholesterol for synthesis of myelin is made locally, not imported into brain. J Neurochem. 1995;64(2):895–901. [PubMed: 7830084]
61. Zhang J, Liu Q. Cholesterol metabolism and homeostasis in the brain. Protein & cell. 2015;6(4):254–64. [PubMed: 25682154]
62. Haberl MG, Zerbi V, Veltien A, Ginger M, Heerschap A, Frick A. Structural-functional connectivity deficits of neocortical circuits in the Fmr1 (-/y) mouse model of autism. Sci Adv. 2015;1(10):e1500775. [PubMed: 26702437]
63. Lai JK, Lerch JP, Doering LC, Foster JA, Ellegood J. Regional brain volumes changes in adult male FMR1-KO mouse on the FVB strain. Neuroscience. 2016;318:12–21. [PubMed: 26794591]
64. Reiss AL, Lee J, Freund L. Neuroanatomy of fragile X syndrome: the temporal lobe. Neurology. 1994;44(7):1317–24. [PubMed: 8035938]
65. Gothelf D, Furfaro JA, Hoeft F, Eckert MA, Hall SS, O'Hara R, et al. Neuroanatomy of fragile X syndrome is associated with aberrant behavior and the fragile X mental retardation protein (FMRP). Ann Neurol. 2008;63(1):40–51. [PubMed: 17932962]

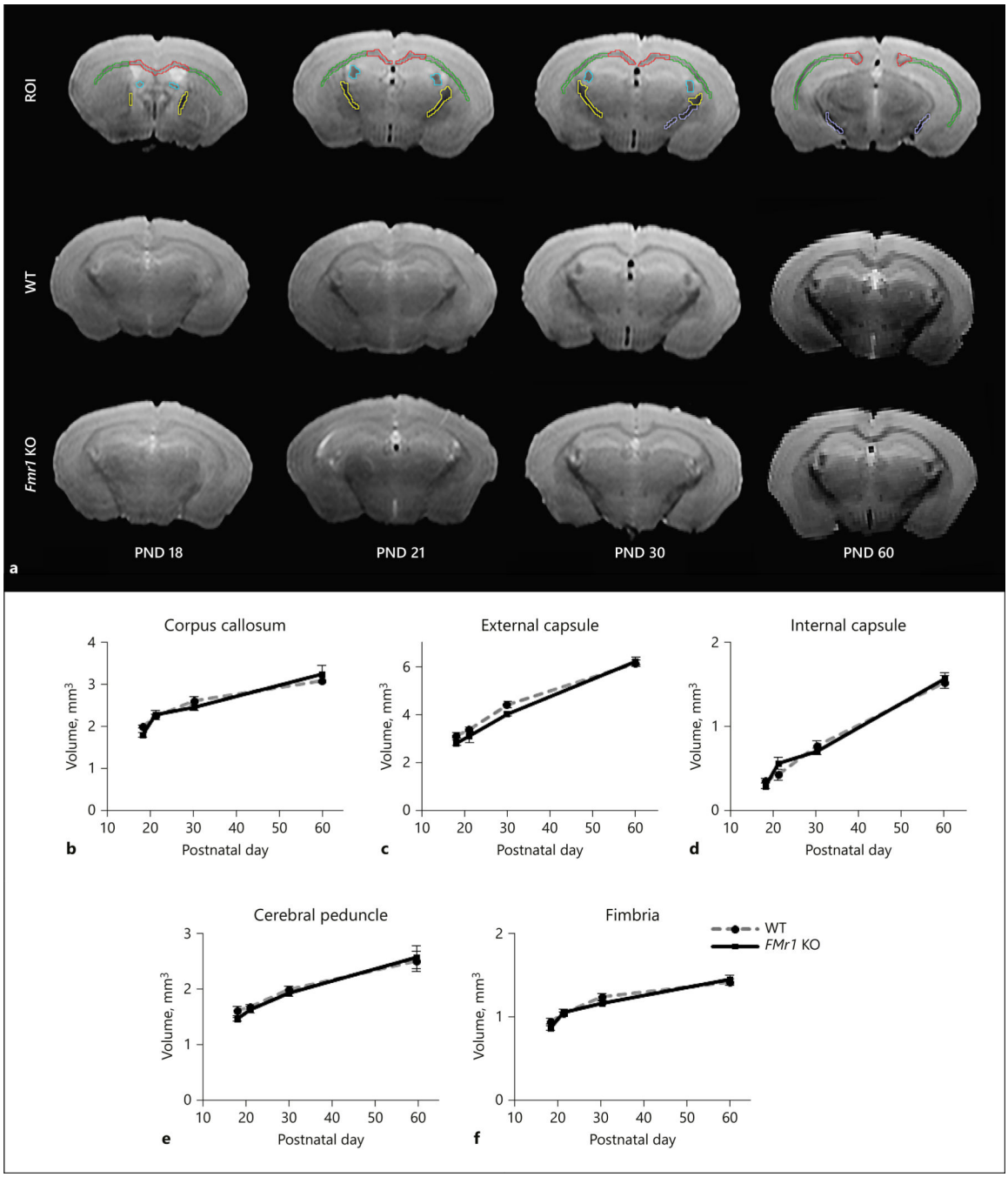

Figure 1:

White matter volume between *Fmr1* KO and WT mouse brains. The representative T_2 images and ROI overlay are shown in 1a. The ROIs show representative white matter regions from WT PND 30 mouse brain, with corpus callosum (red), external capsule (green), internal capsule (yellow), cerebral peduncle (purple), and fimbria (blue). Regional white matter volume (mm^3; mean ± standard error) in the developing WT (gray dashed line) and *Fmr1* KO (black solid line) mouse brains are shown in b) the corpus callosum, c) external and d) internal capsule, e) cerebral peduncle, and f) fimbria. The ages studied were PND 18

(*Fmr1* KO n= 9, WT n=9), 21 (*Fmr1* KO n=12, WT n=14), 30 (*Fmr1* KO n=13, WT n=12), and 60 (*Fmr1* KO n=6, WT n=6). Interaction of (genotype X age) was not significant in white matter regions and the whole brain with respect to volume.

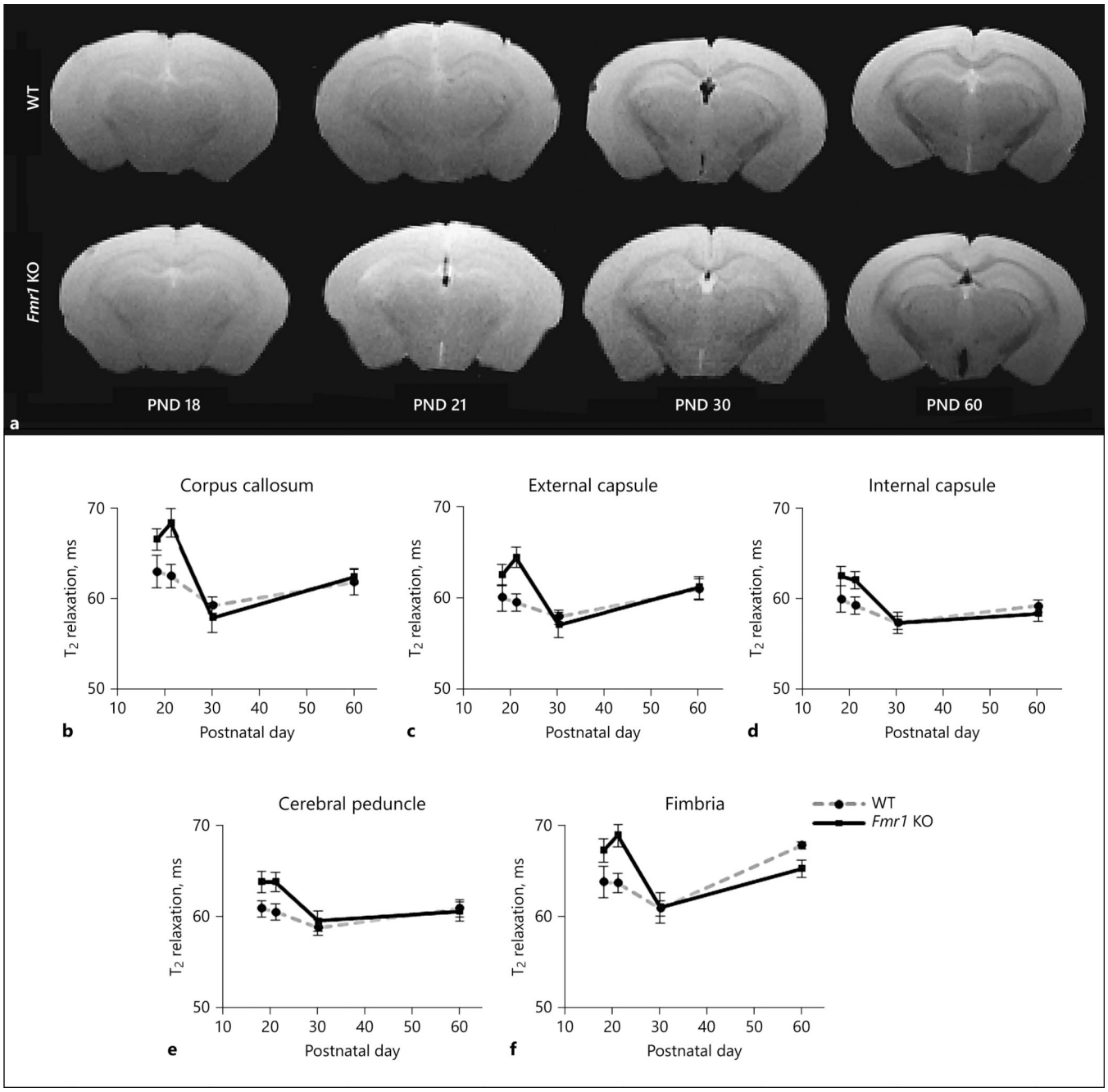

Figure 2:

T_2 relaxation time in white matter regions of the *Fmr1* KO and WT mouse brain. The representative images at TE = 9.3 are shown for *Fmr1* KO and WT mouse brains at each age in 2a. T_2 relaxation time (ms ± standard error) changes in WT (gray dashed line) and *Fmr1* KO (black solid line) mice from PND 18 (*Fmr1* KO n= 9, WT n=9), 21 (*Fmr1* KO n=12, WT n=14), 30 (*Fmr1* KO n=12, WT n=12), and 60 (*Fmr1* KO n=6, WT n=6). Relaxation times were measured in white matter regions of the b) corpus callosum, c) external and d) internal capsule, e) cerebral peduncle, and f) fimbria. No significant (genotype X age) interaction was found in T_2-relaxation.

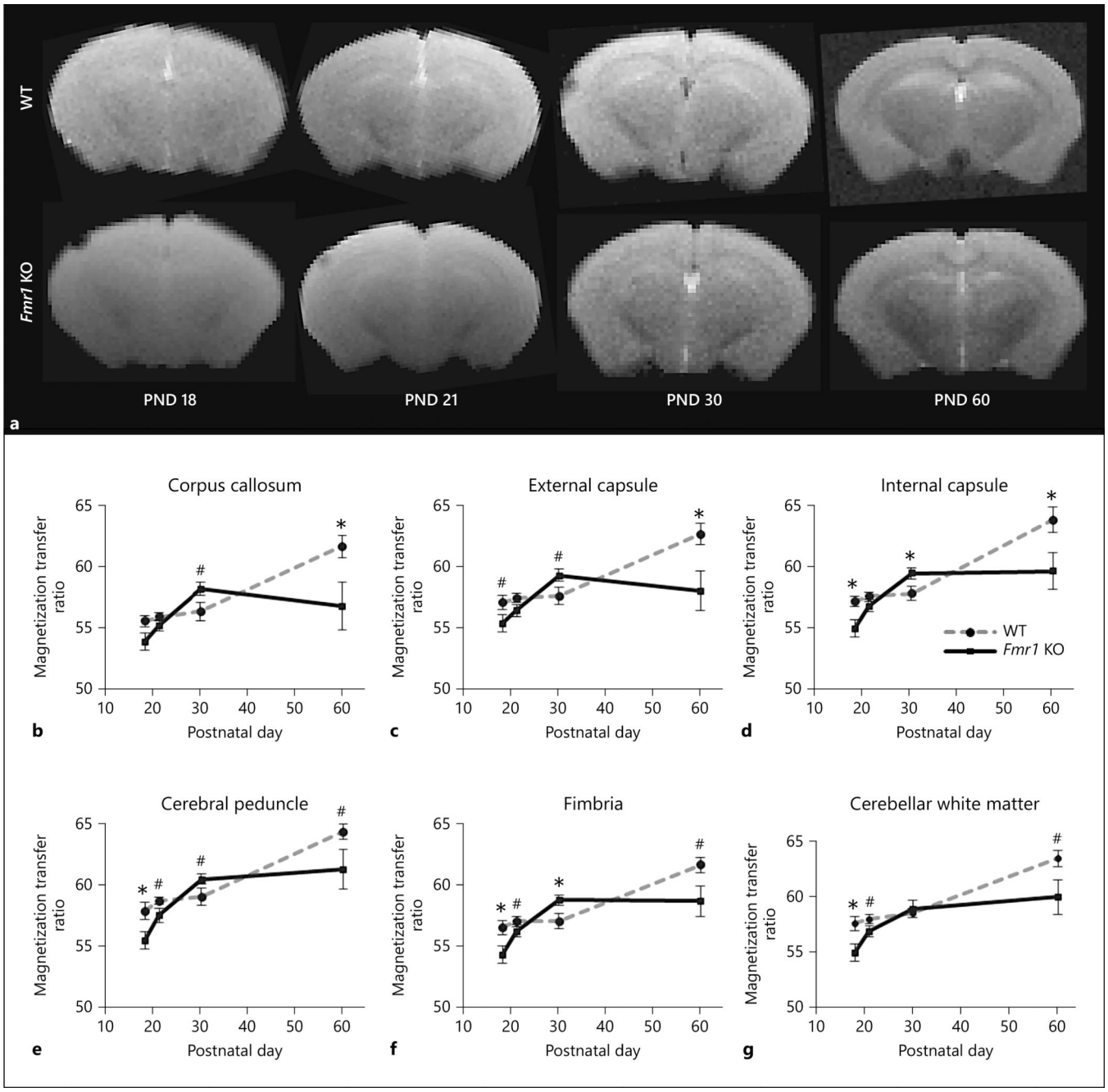

Figure 3:

Magnetization transfer ratio of white matter regions between *Fmr1* KO and WT mouse brains. The representative images at the center frequency of water protons are shown in figure 3a for *Fmr1* KO and WT mouse brains. Magnetization transfer ratio (mean ± standard error) from regional white matter between WT (gray dashed line) and *Fmr1* KO mice (black solid line) in the b) the corpus callosum, c) external and d) internal capsule, e) cerebral peduncle, f) fimbria, and g) cerebellar white matter at PND 18 (*Fmr1* KO n= 9, WT n=9), 21 (*Fmr1* KO n=12, WT n=14), 30 (*Fmr1* KO n=13, WT n=12), and 60 (*Fmr1* KO n=6, WT n=6). A significant (genotype X age) was found in all white matter regions. The significant

genotype differences in MTR between WT and *Fmr1* KO mice are marked with * $p < 0.05$ and # $p < 0.10$.

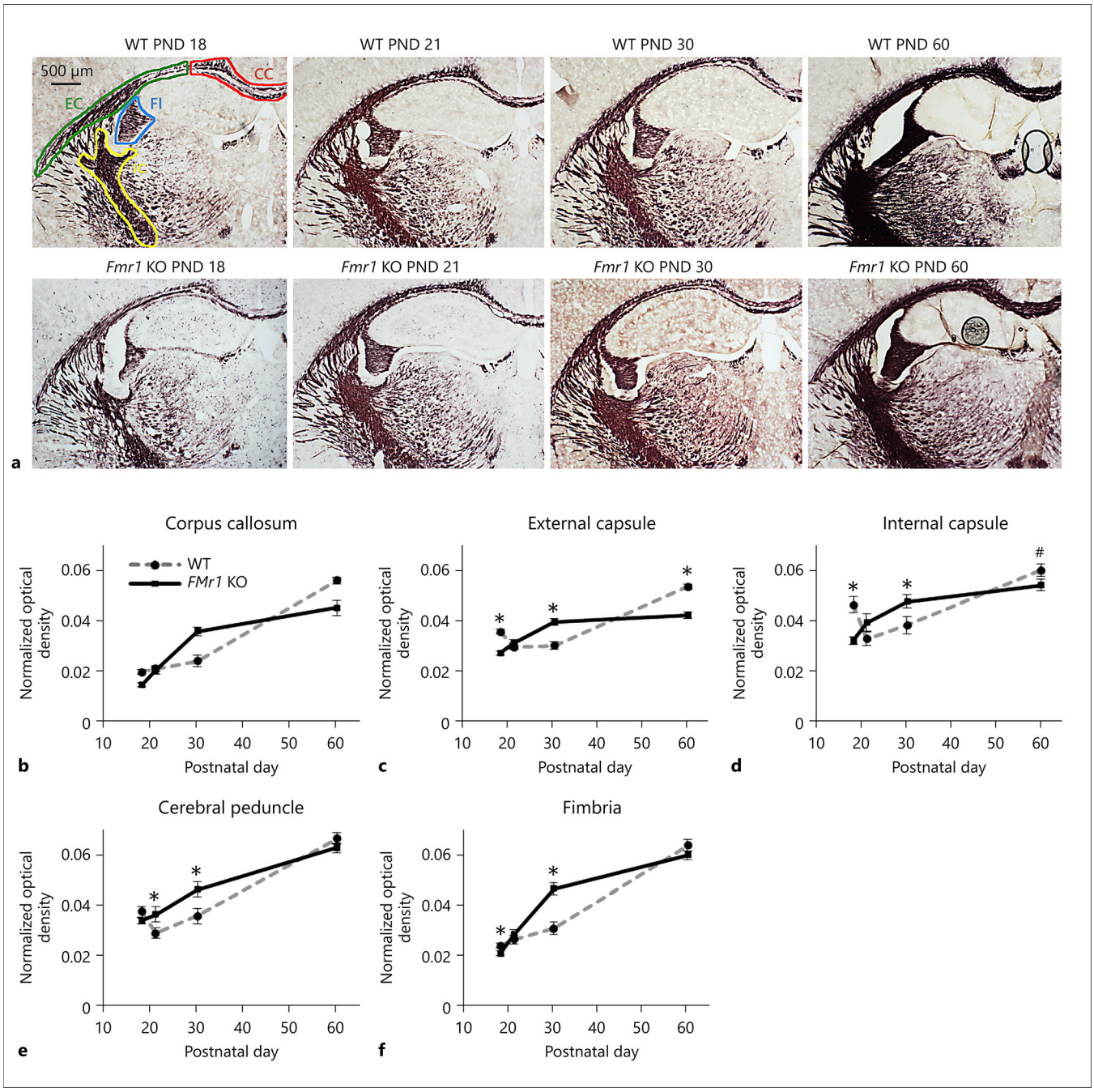

Figure 4:

Myelin density of *Fmr1* KO and WT mouse brains. A) Representative images of myelin staining with Black Gold II in WT and *Fmr1* KO mouse brains. Approximate ROIs are drawn with corpus callosum (CC) in red, external capsule (EC) in green, internal capsule (IC) in yellow, and fimbria (FI) in blue. The cerebral peduncle is not shown but is posterior to the internal capsule. The images were taken between Bregma −1.70 to −2.30 at PND 18 (*Fmr1* KO n= 6, WT n=6), 21 (*Fmr1* KO n=6, WT n=6), 30 (*Fmr1* KO n=6, WT n=6), and 60 (*Fmr1* KO n=6, WT n=6). The scale bar represents 500 μm and is shown in the bottom

left figure. Myelin density was measured by optical density normalized to the area of the ROI. Normalized optical density (mean ± standard error) changes are shown for each ROI including: b) corpus callosum, c) external capsule, d) internal capsule, e) cerebral peduncle and f) fimbria for both genotypes. Significant differences between *Fmr1* KO and WT myelin density were indicated with * $p < 0.05$ and # $p < 0.10$.

Table 1:

Effects and interactions from mixed factor analysis of variance

	DF	Mean square	F-value	p-value
Volume				
Factors				
genotype	1	0.22692	3.276	0.0711
age	3	29.06199	419.556	< **0.0001**
region	4	157.75970	2277.512	< **0.0001**
Interaction				
genotype X age	3	0.33543	4.842	**0.0026**
genotype X region	4	0.05032	0.726	0.5743
age X region	12	3.12447	45.107	< **0.0001**
genotype X age X region	12	0.02929	0.423	0.9542
T_2 relaxation				
Factors				
genotype	1	88.57936	7.704	**0.0058**
age	3	278.51759	24.222	< **0.0001**
region	4	226.09369	19.663	< **0.0001**
Interaction				
genotype X age	3	74.45175	6.475	**0.0003**
genotype X region	4	3.08973	0.269	0.8980
age X region	12	13.86864	1.206	0.2767
genotype X age X region	12	2.10590	0.183	0.9990
Magnetization transfer ratio				
Factors				
genotype	1	162.23418	39.335	< **0.0001**
age	3	348.46606	84.488	< **0.0001**
region	4	73.99728	17.941	< **0.0001**
Interaction				
genotype X age	3	115.37544	27.974	< **0.0001**
genotype X region	4	0.34353	0.083	0.9875
age X region	12	1.96365	0.476	0.9283
genotype X age X region	12	1.01362	0.246	0.9957
Black Gold II staining				
Factors				
genotype	1	0.00057	14.473	**0.0001**
age	3	0.00914	232.284	< **0.0001**
region	4	0.00374	94.993	< **0.0001**

	DF	Mean square	F-value	p-value
Interaction				
genotype X age	3	0.00062	15.798	< **0.0001**
genotype X region	4	0.00016	4.140	**0.0024**
age X region	12	0.00083	21.168	< **0.0001**
genotype X age X region	12	0.00005	1.244	0.2468

Table 2.

Whole brain and normalized white matter volumes in *Fmr1* KO and WT mice.

Whole brain volume					
Mixed factor ANOVA	DF	Mean square	F-value	p-value	
Genotype	1	88.26	0.02004	0.88783	
Age	3	12870.96	2.92260	**0.03986**	
Genotype X age	3	9761.81	2.21661	0.09380	
Means	Age	WT Volume (mm^3)	SE	*Fmr1* KO Volume (mm^3)	SE
	PND 18	352.09	22.64	341.82	5.94
	PND 21	342.47	9.58	376.16	14.71
	PND 30	360.60	5.13	302.66	37.65
	PND 60	387.02	4.72	412.60	15.97
Normalized white matter volume					
Mixed factor ANOVA		DF	Mean square	F-value	p-value
Factors	Genotype	1	0.10400	1.572	0.21100
	Age	3	0.000003	0.006	0.999
	Region	4	1.72600	3555.836	**<0.0001**
Interactions	Genotype X age	3	0.000003	0.006	0.999
	Genotype X region	4	0.00005	0.109	0.979
	Age X region	12	.00625	12.868	**<0.0001**
	Genotype X age X region	12	.00015	0.315	0.987
Means	Region	WT Normalized volume	SE	*Fmr1* KO Normalized volume	SE
PND 18	Corpus callosum	0.294	0.002	0.290	0.014
	External capsule	0.444	0.005	0.452	0.028
	Internal capsule	0.050	0.003	0.047	0.006
	Cerebral peduncle	0.137	0.006	0.135	0.006
	Fimbria	0.076	0.003	0.072	0.004
PND 21	Corpus callosum	0.291	0.005	0.288	0.007
	External capsule	0.435	0.007	0.430	0.007
	Internal capsule	0.055	0.003	0.066	0.004
	Cerebral peduncle	0.138	0.005	0.135	0.006
	Fimbria	0.082	0.002	0.082	0.004
PND 30	Corpus callosum	0.264	0.010	0.266	0.007
	External capsule	0.443	0.010	0.435	0.006
	Internal capsule	0.076	0.005	0.076	0.004
	Cerebral peduncle	0.135	0.003	0.142	0.004
	Fimbria	0.081	0.003	0.082	0.002

PND 60	Corpus callosum	0.227	0.001	0.230	0.008
	External capsule	0.450	0.007	0.444	0.010
	Internal capsule	0.112	0.007	0.112	0.005
	Cerebral peduncle	0.138	0.012	0.139	0.013
	Fimbria	0.074	0.002	0.075	0.003